Application of Ultra-Wideband for the Detection of Intercranial Pulsation

S Panda[1], R K Samantaray[2], T K Mohanta[3]

1.Dept.of Electronics & Communication .Engg, REC, Bhubaneswar, Odisha, India.
2.Dept.of Electronics & Communication .Engg, REC, Bhubaneswar, Odisha, India.
3. Dept.of Electronics & Communication .Engg, Sudhananda Engg & Research center, Bhubaneswar, Odisha, India.
samantaray.ranjan75@gmail.com

Abstract: We have shown the feasibility of UWB radar to detect involuntary head motions in the sub-mm range, demonstrating the feasibility of interfacing a MR scanner with an external UWB radar based motion tracking system. It is well known that simultaneous intracranial oscillation also occur, induced by respiration and myocardial contraction. Hence, it is only consequent to ask whether these oscillations are detectable by UWB radar.
[S Panda, R K Samantaray, T K Mohanta. **Application of Ultra-Wideband for the Detection of Intercranial Pulsation.** *Researcher* 2013;5(4):55-58]. (ISSN: 1553-9865). http://www.sciencepub.net/researcher. 10

Keywords: Ultra-Wideband (UWB), Magnetic resonance imaging (MRI); cardiology

I. INTRODUCTION

Magnetic resonance imaging (MRI) is the most important tool in modern cardiology and neuroscience. Due to the continuing improvements of the spatial and temporal resolution of this imaging modality, great progress could be made in the field of brain science and the imaging of cardiovascular diseases. Nowadays, however, a point has been reached where further improvements in resolution are limited. The signal to noise ratio in MRI increases approximately linearly with increasing static magnetic field, therefore the use of so-called high ($B_0 \geq 3$ T) and ultra-high field ($B_0 \geq 7$ T) systems can overcome these limits and facilitate new findings about the human brain and the heart. Our research aims at the synergetic use of ultra-wideband (UWB) sounding combined with MRI, to gain complementary information, e.g. to accelerate and improve cardiac and cranial MRI. Physiological noise like respiratory and cardiac displacements introduce motion artifacts in the MR image. With an Mrcompatible UWB radar, the characteristic landmarks of the heart muscle, the thorax or the brain/skull during breathing and cardiac activity could be followed without disturbing the actual MR measurement. We have already established a combined MRI / UWB prototype demonstrating the absence of any mutual interference between both systems, proving the feasibility of the UWB radar method to monitor respiratory and myocardial displacements in a 3 T scanner [1]. In a further study we have shown the feasibility of UWB radar to detect involuntary head motions in the sub-mm range.

All kinds of involuntary motions became visible (respiratory, cardiac), even doze-off-events were visible, demonstrating the feasibility of interfacing a MR scanner with external UWB radar based motion tracking system [2]. It is well known that simultaneous intracranial oscillation also occurs induced by the same physiological sources mentioned above [3]. Hence, it is only consequent to ask whether these oscillations are detectable by UWB radar. Due to the simultaneous occurrence of the

intracranial displacement and the vibration of the whole head, decomposing both signals requires sophisticated methods. As an initial step towards the solution of this challenge we need to get a feeling of the change which is introduced in the acquired reflection signal by an intracranial oscillation when exposing the human head to ultra-wideband electromagnetic signals. To this end we applied an analytical approach [4] which models the signal path and the oscillating stratified arrangement of the brain to get signals free of any interfering compositions.

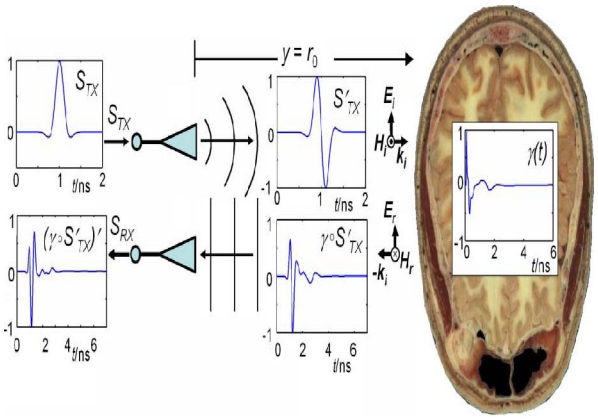

Fig. 1. Sketch of the signal path model for the current transfer function S_{Rx}/S_{Tx} = I_{Rx}/I_{Tx}. S_{Tx}: excitation signal. $S'_{Tx} = E_i$: free space signal in the channel. Planar linearly polarized electromagnetic wave: E_i/E_r, H_i/H_r: incident/reflected electrical/magnetical field component. k_i: wave vector of the incident wave. γ: impulse response function (IRF) of the multi-layered dielectric structure. $\gamma \circ S'_{Tx} = Er$: reflected electrical field component. $S_{Rx}=(\gamma \circ S'_{Tx})'$: received current signal/pulse. There o represents the convolution operator. Anatomic slice of the human head taken from [5].

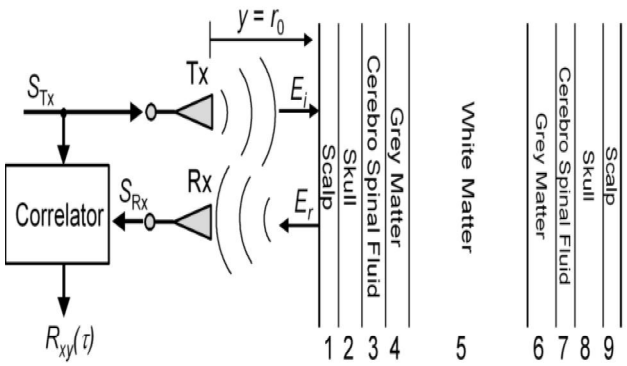

Fig. 2. UWB radar probing a multilayered dielectric structure (bi-static setup). S_{Tx}/S_{Rx}: transmitted/received signal; Tx/Rx: transmit/receive antenna; E_i/E_r: incident/reflected electrical field component; $R_{xy}(\tau)$: correlation result from UWB device.

II. THE MODEL APPROACH

Figure 1 and, in a more abstracted way, Fig. 2 depict the set-up commonly used to probe the human body with a UWB device. The antennas are co-polarized and the normal incidence of the EM-wave is assumed. The body can be assumed to form a multilayered dielectric structure with a characteristic reflection coefficient $\Gamma(\omega)$. The UWB signal, which can be a pulse or a pseudo-noise sequence of up to 10 GHz bandwidth, is transmitted utilizing appropriate pulseradiating antennas Tx (e.g., horn or tapered slot antennas). The reflected signal is detected by Rx and calculating the correlation between received signal S_{Rx} and transmitted signal pulse S_{Tx} is usually the first step in further signal-processing. We model the human head from 9 planar isotropic dielectric layers, those arrangement as well as individual thicknesses approximate a trans-cranial slice from the Visual Human data set [5] (Fig. 1, and Fig.2). The spectral response of a dielectric medium is appropriately described in terms of multiple Cole-Cole dispersion which, with a choice of parameters appropriate to each constituent, can be used to predict the

dielectric behavior over the desired frequency range [6]. For such a layered arrangement the reflection response $\Gamma(\omega)$ can be recursively calculated using an iterative formulation published by [7]. In this way the response of $\Gamma(\omega, t)$ to the variation of a certain internal interface can be analyzed. If the stratified object is located at a distance r0 from the Tx/Rx antennas, which are assumed to be positioned in their mutual far-field, the ratio of the E-fields in the frequency domain at Rx and Tx becomes, assuming a TEM-wave [4]:

$$\frac{E_{Rx}}{E_{Tx}}(\omega) = \Gamma(\omega) \times \left(a(r_0) \times \exp\left(-2j\frac{\omega r}{c_0}\right)\right) \sim (S_{Rx}/(j\omega)^2 S_{Tx})(\omega) \text{ --------(1)}$$

To account for the path dependent damping of the electromagnetic wave in the far-field $a(r_0)$ is introduced. Assuming a spherical wave reflected at a plane, extended surface, $a(r_0) = (2r_0)^{-1}$. A typical class of broadband electromagnetic excitation pulses are those of the Gaussian shape and their derivatives [8]. We used a modified Ricker pulse, which is the second derivate of the Gaussian pulse. A broadband pulse, whose spectral behavior is similar to the excitation signal we apply in our envisaged medical application (flat spectrum down to several MHz, -3dB at 10 GHz), can be formed from the so called Ricker pulse (Fig.1, S_{Tx}). Theoretically the received signal S_{Rx} in the frequency domain becomes (Fig.2) [4]:

$$S_{Rx} = [S_{Tx}H_{Tx}H_{Rx}\Gamma(\omega,t) \times a(r_0)\exp(-2(r_0)j\omega/c_0)] \text{ ----------(2)}$$

with H_{Tx}, H_{Rx} are the transfer function of the transmitting and receiving antenna, respectively.

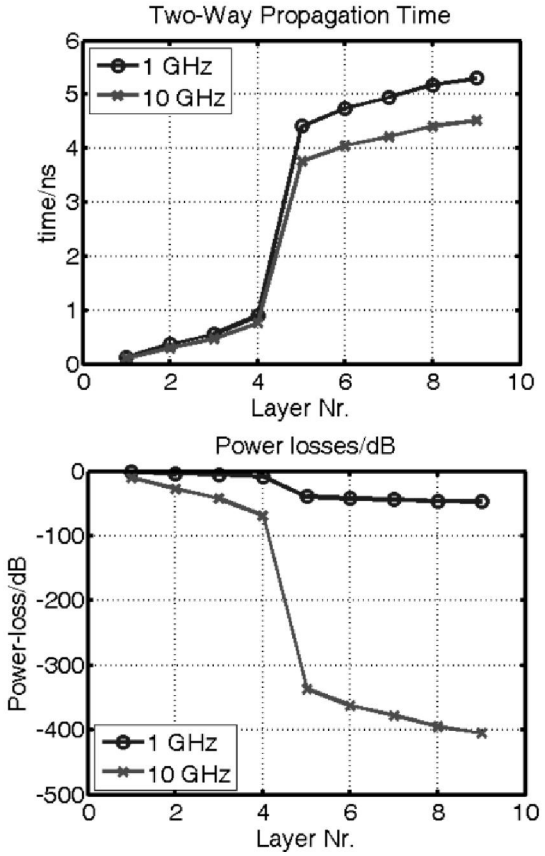

Fig.3. Two-way propagation time and one-way power losses of the layered human head model: *Left:* calculated propagation time after each layer for 2 different frequencies. Propagation times to reach a certain interface are indicated by the data points. The lines are guides to the eye. *Right:* power losses after each layer of the electromagnetic wave while traversing the 9- layer model computed for two different frequencies.

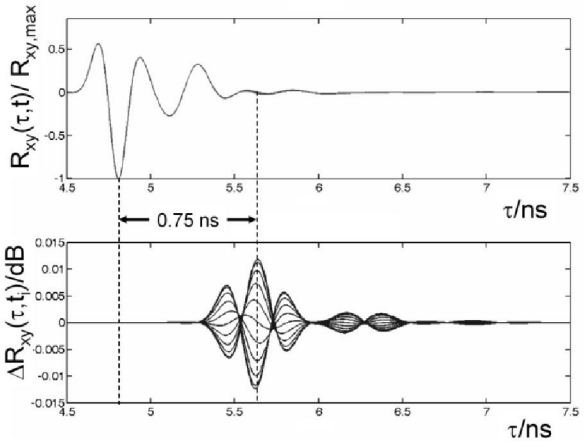

Fig.4. *Upper*: normalized overlapped correlation results $R_{xy}(\tau,t)/R_{xy,max}$ gained from a sinusoidal oscillation of the intracranial white matter (10 discrete time steps per period). *Lower*: overlapped variation $\Delta R_{xy}(\tau,t_i)$ in $R_{xy}(\tau)$ for each elongation, i.e. each time step t_i. The envelope of ΔR_{xy} corresponds to a 1 mm elongation. Indicated by Δt = 0.75 ns is the two-way propagation time below the surface of the model where the maximum is found.

III. RESULTS

From the layered model we can calculate the evolution of the propagation time and power losses while the electromagnetic wave traverse each layer at different frequencies (s. Fig. 3). The two-way propagation time to reach layer 5, i.e. the white matter, is $\tau_5 \sim 0.7$ ns (s. Fig.3, left). In the following we will simulate the physiological event by variations of $\Gamma(\omega, t)$, which is done by a sinusoidal oscillation of the white matter (layer 5) by an amplitude of 1 mm. Accordingly, the Cerebro Spinal Fluid (CSF, layer 3 and layer 7) varie antipodal. The calculated correlation result $R_{xy}(\tau,t)$ gained from the simulation and the variation $\Delta R_{xy}(\tau,t_i)$ after a certain propagation time are depicted in Fig.4. For a maximum intracranial amplitude of 1 mm the variation becomes $\Delta R_{xy}(\tau,t_i) \sim 0.01$ dB at a propagation time where the white matter is located ($\tau_{5*} \sim 0.7$ ns, s. Fig.4). Hence, requesting a high-fidelity receiver. The reconstruction of the intracranial motion applying the reconstruction algorithm proposed in [4] gave us a maximum deviation from the reference oscillation of about 4%.

REFERENCES

[1] F. Thiel, M. Hein, U. Schwarz, J. Sachs, F. Seifert, Rev. Sci. Instrum, vol. 80, issue 1, NY, AIP, ISSN 0034-6748, (2009)

[2] F. Thiel, Hein M, Sachs J, Schwarz U, Lindel T D, Seifert F, Proc. Intl. Soc. Mag. Reson. Med. 17, (ISMRM), p. 4548, (2009).

[3] D. A. Feinberg, A. S. Mark, Radiology, 163, 793-799, (1987).

[4] F. Thiel and F. Seifert, J. Appl. Phys., vol. 105, issue 4, (2009).

[5] THE VISIBLE HUMAN PROJECT, U.S. NATIONAL LIBRARY OF MEDICINE, 8600 ROCKVILLE PIKE, BETHESDA, MD 20894.

[6] S. Gabriel et al., Phys. Med. Biol., 41, 11, 2251-2269, 2271-2293 (1996)

[7] S. J. Orphanidis: Electromagnetic Waves and Antennas, p. 118, Rutgers University, ISBN 978-0-9793713-2-5, (2008).

[8] M. Hämäläinen, Singleband UWB systems, Academic Dissertation University of Oulu, pp. 32-35, (2006).

3/24/2013